AIP Applied Physics Letters

Room temperature ultraviolet GaN metal-coated nanorod laser

Yu-Cheng Hsu, Kuok-Pan Sou, Shih-Pang Chang, Kung-Shu Hsu, M. H. Shih, Hao-Chung Kuo, Yuh-Jen Cheng, and Chun-Yen Chang

Citation: Applied Physics Letters **103**, 191102 (2013); doi: 10.1063/1.4828997
View online: http://dx.doi.org/10.1063/1.4828997
View Table of Contents: http://scitation.aip.org/content/aip/journal/apl/103/19?ver=pdfcov
Published by the AIP Publishing

Articles you may be interested in

GaN based nanorods for solid state lighting
J. Appl. Phys. **111**, 071101 (2012); 10.1063/1.3694674

High-Q (>5000) AlN nanobeam photonic crystal cavity embedding GaN quantum dots
Appl. Phys. Lett. **100**, 121103 (2012); 10.1063/1.3695331

Room temperature lasing with high group index in metal-coated GaN nanoring
Appl. Phys. Lett. **99**, 251111 (2011); 10.1063/1.3671648

Lasing in metal-coated GaN nanostripe at room temperature
Appl. Phys. Lett. **98**, 131110 (2011); 10.1063/1.3572023

Room temperature laser action from multiple bands in photoexcited GaN grown on a silicon substrate
Appl. Phys. Lett. **90**, 151116 (2007); 10.1063/1.2722201

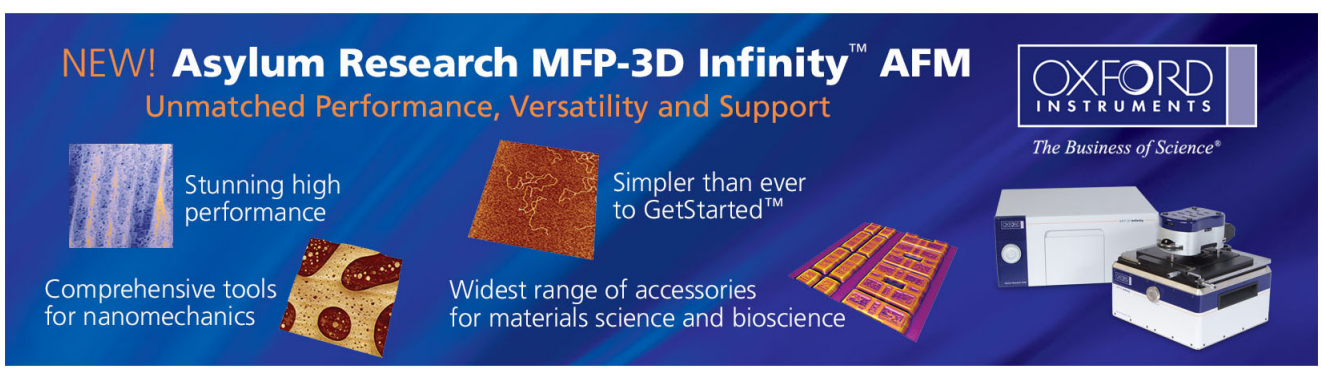

This article is copyrighted as indicated in the article. Reuse of AIP content is subject to the terms at: http://scitation.aip.org/termsconditions. Downloaded to IP: 140.113.38.11 On: Wed, 30 Apr 2014 08:43:22

Room temperature ultraviolet GaN metal-coated nanorod laser

Yu-Cheng Hsu,[1] Kuok-Pan Sou,[2] Shih-Pang Chang,[2] Kung-Shu Hsu,[2,3] M. H. Shih,[2,3,a)] Hao-Chung Kuo,[2] Yuh-Jen Cheng,[2,3] and Chun-Yen Chang[1]
[1]*Department of Electronic Engineering, National Chiao Tung University, 1001 Ta Hsueh Rd., Hsinchu 300, Taiwan*
[2]*Department of Photonics & Institute of Electro-Optical Engineering, National Chiao Tung University, 1001 Ta Hsueh Rd., Hsinchu 300, Taiwan*
[3]*Research Center for Applied Sciences, Academia Sinica, Taipei 11529, Taiwan*

(Received 18 June 2013; accepted 21 October 2013; published online 4 November 2013)

This study demonstrates a room-temperature ultraviolet GaN/Al nanorod (NR) metal laser with an optimized sidewall. A wet-chemical etching process with potassium hydroxide was used to control the GaN NR sidewall angle and polish the NR surface. The lasing action was observed near a wavelength of 365 nm with a low threshold power density of 5.2 mJ/cm^2. The high-quality factor (Q) surface plasmon lasing modes were characterized with experiments and three-dimensional finite-element method simulations. We also studied the optical modes in GaN metal-coated NR with and without an Al layer and verified the metal layer is necessary for high-Q resonant modes.
© *2013 AIP Publishing LLC*. [http://dx.doi.org/10.1063/1.4828997]

In recent years, a substantial amount of research has been conducted in minimizing optical cavities to achieve nanoscale lasers used for chip-scale photonic integrated circuits. The metal-cladding semiconductor laser is one of the most promising schemes for breaking the optical diffraction limit because of surface plasmon (SP) effects.[1,2] Semiconductor metal lasers with different cavities,[3–17] including nanodisks, nanowires, nanorings, and other structures, have been demonstrated. However, most reported metal nanolasers can operate only in a cryogenic condition because of the high optical losses with the metal and the low quality factor (Q) value. In addition, wide-band-gap III-nitride (aluminum gallium indium nitride, AlInGaN) semiconductor alloys have attracted a substantial amount of attention as potential platforms for high-frequency and high-power electronics,[18] visible light-emitting diodes (LEDs),[19,20] and ultraviolet (UV)-wavelength lasers and bio-sensors.[21,22] Few studies have demonstrated the fabrication of UV GaN-based metal nanolasers with an epitaxially grown metal layer[13] and metal nanocavities at room temperature.[16,17] However, the surface and sidewall qualities are key factors for achieving high-performance metal nanolasers because of their compact cavities and ultra-small mode profiles.[13] The tiled angle and rough sidewall in a metal-semiconductor cavity might degrade the optical confinement and increase optical loss, leading to poor emission quality, especially for such small semiconductor-metal cavity. In this study, we demonstrate a large-area UV GaN-based nanorod (NR) metal laser by using the nanoimprint lithography (NIL) technique and optimizing the NR cavity sidewall. A large-area and uniform GaN NR structure was produced using the NIL technique, and the NR tiled angle was optimized and the NR sidewall was polished by performing extra chemical etching with potassium hydroxide (KOH). Because of the sharp sidewall angle and smooth surface, room-temperature, low-threshold lasing action was achieved from the GaN NR metal cavity.

To understand the optical loss in the metal nanorod cavity caused by the sidewall angle, we investigated GaN metal NR cavities with different sidewall tiled angles. Fig. 1(a) shows the GaN metal NR cavities with different sidewall tiled angles ($\theta = 90°$ and $\theta < 90°$). The three-dimensional (3D) finite-element method (FEM) was applied to perform the simulation of the metal NR cavities. Fig. 1(b) shows the simulated top view and cross-sectional view mode profiles as well as the Q of the GaN metal NR cavities with sidewall tiled angles of $\theta = 90°$, $\theta = 89°$, and $\theta = 84°$, respectively. A well-confined optical mode with a high Q value of 127 was observed in the NR with a sidewall angle of $\theta = 90°$. However, the mode's confinement decreased and its Q value dropped from 127 to 45 when the NR sidewall angle decreased from $\theta = 90°$ to 89°. The degradation of this optical mode in the metal NR cavity intensified (Q = 36) when the sidewall tiled angle reached $\theta = 84°$, which was the tiled sidewall angle of GaN NR after the dry etching step was performed without sidewall optimization. The results clearly show that the optical confinement in this compact GaN metal NR cavity strongly depended on the sidewall angle. Therefore, controlling the metal NR sidewall angle is critical to achieving room-temperature lasing. To obtain a high-Q GaN metal NR cavity, the sidewall angle of the GaN metal NR was optimized to 90° by adding an extra chemical etching step during the device fabrication process.

The metal-clad GaN NRs were implanted on a 2-μm-thick c-plane (0001) GaN layer on a sapphire substrate, which was grown using metal-organic chemical vapor deposition (MOCVD). Fig. 2 shows a schematic diagram of the procedures used for fabricating the metal-clad GaN NR structure. First, a 0.5-μm-thick SiO_2 layer was deposited as an etching mask, and the NR patterns were defined using the NIL technique.[23,24] After dry etching with inductively coupled plasma reactive ion etching (ICP-RIE) and removing the mask residue, trapezoid-type GaN NRs with an approximate height of 1.2 μm were obtained. Subsequently, an additional sidewall optimization with a KOH-based etchant was

a)mhshih@gate.sinica.edu.tw

 © 2013 AIP Publishing LLC

This article is copyrighted as indicated in the article. Reuse of AIP content is subject to the terms at: http://scitation.aip.org/termsconditions. Downloaded to IP: 140.113.38.11 On: Wed, 30 Apr 2014 08:43:22

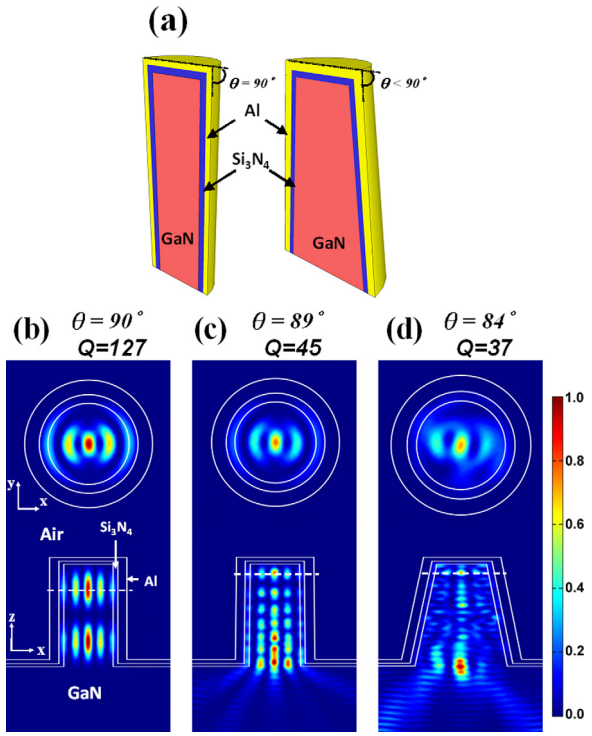

FIG. 1. (a) Schematic diagram of the metal-cladded GaN NR structure with cylindrical-type, $\theta = 90°$ (left) and Trapezoid-type, $\theta = 84°$ (right). Calculated Al-cladded GaN NR electric field intensity $|E|^2$ distribution in the top view (upper panel) and side view (lower panel) (b) $\theta = 90°$, denote as M_2^{90}. (c) $\theta = 89°$, denote as M_2^{89}. (d) $\theta = 84°$, denote as M_2^{84}. The top view mode profile was calculated at the white dotted surface in the side view.

introduced to achieve smooth cylindrical-type GaN NRs. This unique technique was used to repair the sidewall tiled angle and smooth surface roughness that were caused by the previous bombardment etching process.[25] The tiled sidewall and rough NR surface increased the cavity loss, degraded the quality factor, and increased the threshold. Because the high lasing threshold prohibits laser operation at room temperature, this sidewall optimization step is critical for GaN metal NR lasers. Figs. 3(a) and 3(b) show the scanning electron microscope (SEM) images of the GaN NRs before and after the extra sidewall optimization step was conducted with the KOH etchant for 30 min at 70 °*C*. Before the step, the GaN NRs in Fig. 3(a) had a sidewall tiled angle of 84° and an extremely rough sidewall surface. Cylindrical-type GaN NRs with a diameter of 300 nm and a sidewall angle of 90° were obtained after this step, and are shown in Fig. 3(b). Figs. 3(c) and 3(d), which are magnified SEM images of the GaN NRs in Figs. 3(a) and 3(b), show the differences in the details of the GaN NR sidewalls before and after the KOH etching treatment. In a hexagonal crystalline system, GaN has a stable m-plane $\{10\bar{1}0\}$ that must serve as the etching stop plane.[26] The c-plane GaN NR sidewall surface was the m-plane, which was perpendicular to the GaN template surface. Therefore, the chemical etching step can be performed to support the sharp m-plane sidewall surface, yielding a 90° sidewall angle. In addition to sidewall angle optimization, chemical etching was used to smooth the sidewall surface, which improved the lasing performance of the GaN metal NR laser. Additional details of the sidewall optimization process are described in the supplement document.

After the sidewall optimization step, a 35-nm-thick silicon nitride (Si_3N_4) layer and a 50-nm-thick Al layer were uniformly coated on the GaN NR surface by using plasma-enhanced chemical vapor deposition (PECVD) and electron beam evaporation, respectively. The Al layer exhibited high reflectivity at the UV spectral region, which provided excellent resonance within the GaN nanocavities.[16,17]

The photoluminescence (PL) characterization system contained a 355-nm triple Nd:YAG pulse laser, which was employed as an excitation source at room temperature. The pulse width was 0.5 ns, and the pulse repetition rate was 1 kHz. The spot size of the normal incident beam was approximately 50 μm when using a 15× microscopic objective lens focused on the sample surface. The devices were directly pumped from the metal side of the sample to prevent enormous absorption from the GaN substrate (energy band gap of approximately 3.4 eV) beneath the NRs. The emission signals were collected using the same objective lens and coupled into a multimode fiber, which was connected to an optical spectrometer with a nitrogen-cooled charge-coupled device (CCD) array detector.

Fig. 4(a) shows the room-temperature lasing spectrum of the GaN NR metal cavity, which exhibited three clear emission peaks at wavelengths of 362.5 nm, 364.3 nm, and 365.2 nm denoted M_1^{90}, M_2^{90}, and M_3^{90}, respectively. The light-in-light-out characteristics of mode M_3^{90} are shown in the black curve in Fig. 4(b), and the threshold power density of the mode was approximately 5.2 mJ/cm^2. The blue curve

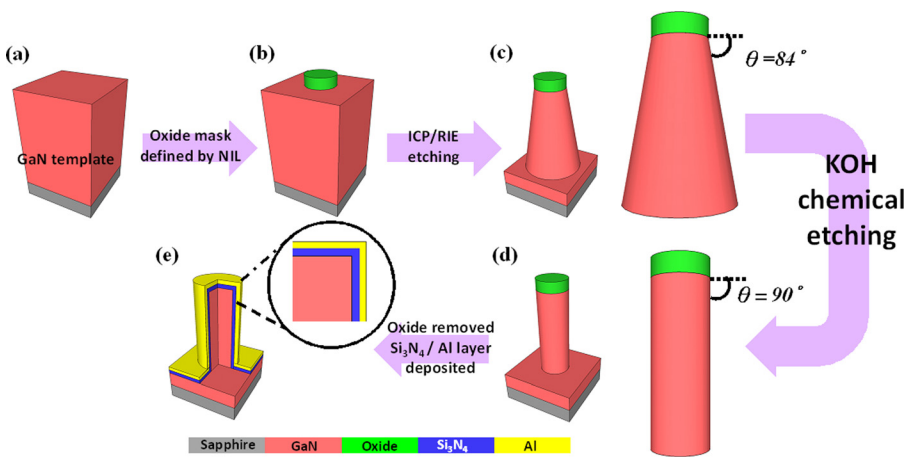

FIG. 2. Schematic diagram process flow of the metal-cladded GaN NR arrays. (a) GaN template on sapphire substrate. (b) Oxide disk arrays as the hard mask which pattern defined by nanoimprint lithography. (c) Trapezoid-type GaN NR arrays to take shape after ICP-RIE process. (d) After KOH chemical etching acquired cylindrical-type GaN NR arrays. (e) After residue oxide removed, Si_3N_4 and Al layer was conformal capping on the cylindrical-type GaN NR arrays by PECVD and E- gun evaporation, respectively.

This article is copyrighted as indicated in the article. Reuse of AIP content is subject to the terms at: http://scitation.aip.org/termsconditions. Downloaded to IP: 140.113.38.11 On: Wed, 30 Apr 2014 08:43:22

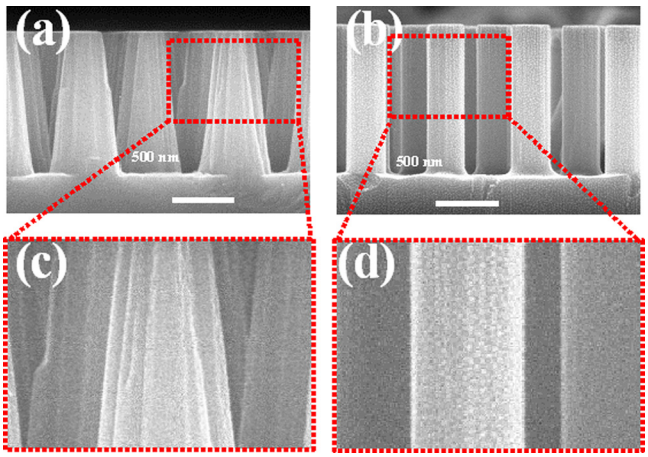

FIG. 3. The SEM image (cross-section) of GaN NR arrays which pattern defined by nanoimprint lithography and etched by ICP-RIE. (a) Trapezoid-type, after ICP-RIE. (b) Cylindrical-type, after ICP-RIE and KOH chemical etching. (c), (d) were magnified the red dotted square within the image of (a) and (b), respectively.

in Fig. 4(b) shows the recorded linewidths pumped at various power densities. The linewidth-narrowing behavior was observed near the threshold, which verified the lasing action of the metal NR laser.

To understand the observed lasing modes, the 3-D FEM was implemented to perform a simulation of the GaN NR metal cavity. The GaN NR structure with a diameter of 300 nm, a height of 1200 nm, a 35-nm-thick Si_3N_4 layer, and a 50-nm-thick Al layer was employed in this simulation. The three high-Q modes were obtained based on the simulation and correspond to the three lasing modes used in the experiment. Fig. 4(c) shows the calculated Q value and the resonant wavelengths of the three resonant modes. The calculated quality factors of the three modes were approximately $M_1^{90} = 119$, $M_2^{90} = 127$, and $M_3^{90} = 136$.

Figs. 4(d)–4(f) show the simulated electric field intensity ($|E|^2$) in the side-view (x–z plane) and top-view (x-y plane) distribution of the three resonant modes in the GaN metal NR. Each top view of the field profile for modes M_1^{90}, M_2^{90}, and M_3^{90} was calculated at the white dotted surface in the side view. The characteristics of the modes appeared within the GaN NRs and around the interface between the NR and the dielectric layer. The mode M_1^{90} was a whispering-gallery (WG)-like SP polariton mode, and the electric field directions were perpendicular to the NR sidewall and the metal surface with an azimuthal mode number of 4, which is shown in Fig. 4(d). The modes M_2^{90} and M_3^{90} show dipole-like resonant mode profiles, as shown in Figs. 4(e) and 4(f). In the two dipole-like mode profiles, the electric field maxima of the modes were located inside the NR center and away from the coated Al metal layer. Therefore, the modes M_2^{90} and M_3^{90} exhibited higher Q values than did the mode M_1^{90}. All three resonant modes had well-confined optical profiles along the z-direction, which indicates that the upper metal layer on the top of NRs improves the vertical optical confinement. To compare the GaN metal NRs fabricated with and without sidewall optimization in the experiment, we also fabricated a GaN metal NR cavity without sidewall optimization as a reference device. Room-temperature lasing

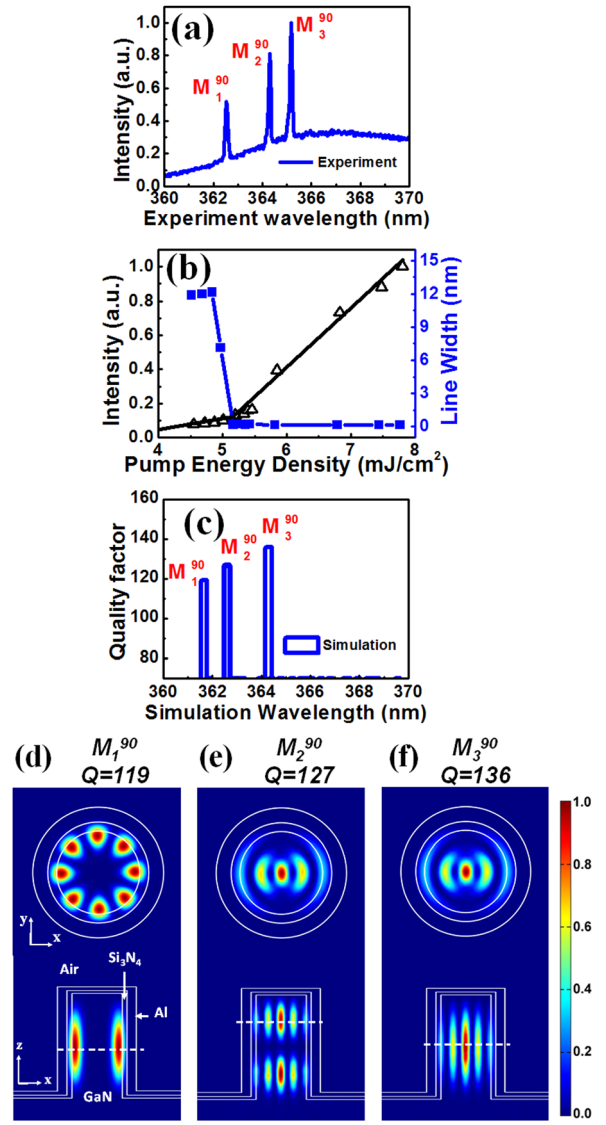

FIG. 4. (a) Light-in light-out curve (L-L curve) of Al-cladded GaN nanorods and linewidth of the lasing peak at 365.2 nm. (b) PL characteristics for Al-cladded GaN NR arrays and (c) used finite element method simulation result. Calculated Al-cladded GaN NR electric field intensity $|E|^2$ distribution in the top view (upper panel) and side view (lower panel) (d) TM-like surface plasmon polariton (SPP) mode (M_1^{90}). (e) TE-like electric dipole mode (M_2^{90}) with z-direction oscillating mode number, n = 2. (f) TE-like electric dipole mode (M_3^{90}) with z-direction oscillating mode number, n = 1. The top view mode profile was calculated at the white dotted surface in the side view.

action was not observed in the NR with a tiled sidewall and a rough surface within the supported power range of the pumping laser.

Because the metal plays a crucial role in improving optical confinement in NR cavities, comparing GaN NR cavities with and without an Al metal layer is worthwhile. Fig. 5 shows the simulated mode profiles and calculated Q values of the GaN NR cavities with and without the Al metal cladding layer. The optical mode in the GaN NR cavity without metal showed leakage to the bottom substrate, which led to a low Q value of 77. The metal-coated NR structure formed a 3D cavity, resulting in a confined resonant mode that was strong within the GaN NR and did not propagate beneath the GaN template and the air region. Therefore, the resonant mode in the metal-coated NR cavity exhibited good optical

This article is copyrighted as indicated in the article. Reuse of AIP content is subject to the terms at: http://scitation.aip.org/termsconditions. Downloaded to IP: 140.113.38.11 On: Wed, 30 Apr 2014 08:43:22

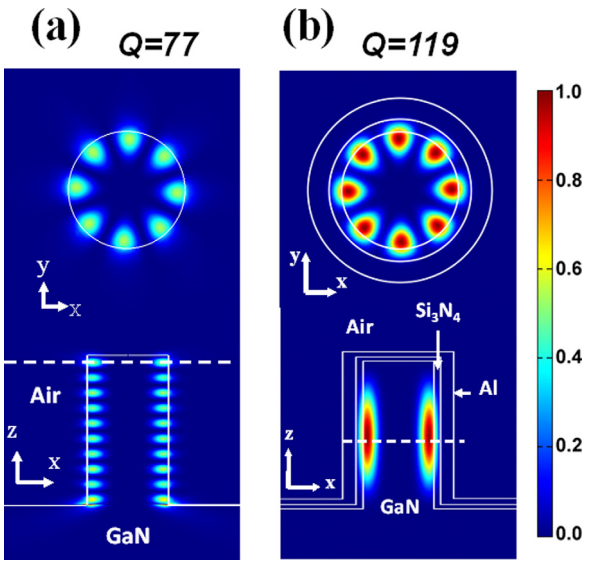

FIG. 5. Calculated Al-cladded GaN NR electric field intensity $|E|^2$ distribution in the top view (upper panel) and side view (lower panel) (a) Pure GaN NR resonator. (b) Metal-cladded GaN NR resonator.

confinement and a high-Q (Q = 119) mode within the UV wavelength range. The metal-coated cavity Q was two times that of the pure GaN resonator in the comparable WG mode (WGM). The enhanced confinement ability enabled the metal-cladded cavities to yield a low-threshold power density, increased the transition from spontaneous to amplified, and stimulated the emission probability. However, the metal-cladded layer caused energy loss from joule heating because of the small resonant mode volume overlap with the sidewall metal layer. Nevertheless, the overall lasing performance was superior to that of the layer without metal-cladded resonators, which exhibited severe optical loss with the same size cavity.

In this study, the fabrication of a large-area UV GaN metal NR laser at room temperature is demonstrated. GaN metal NR cavities with different sidewall angles were studied. By adding an extra chemical etching process, the sidewall angle of the GaN NR was optimized to 90°, minimizing the optical loss and increasing the Q value. When the Al metal layer was used to form a nanocavity, the well-confined resonant mode was observed within the GaN NR, which was theoretically realized by implementing FEM in the simulation. The lasing wavelength was observed at approximately 365 nm, which has a low threshold power density of 5.2 mJ/cm^2 at room temperature. The high-Q SP lasing modes were characterized using experiments and 3D FEM simulations, and the high-symmetry mode profiles are presented. The GaN NR cavities with and without the Al metal layer were also studied. The results indicate that the metal enhanced the optical confinement twofold in the GaN NR cavity.

The authors are grateful to the Center for Nano Science and Technology in National Chiao Tung University (NCTU) for instrument supports. This work is supported in part by the National Science Council, Taiwan under the grant number NSC 102-2112-M-001-019-MY3, Nano-Project granted by Academia Sinica and the 2013 NCTU-RCAS joint project.

[1]V. J. Sorger and X. Zhang, Science **333**, 709 (2011).
[2]D. K. Gramotnev and S. I. Bozhevolnyi, Nat. Photonics **4**, 83 (2010).
[3]M. T. Hill, Y.-S. Oei, B. Smalbrugge, Y. Zhu, T. de Vries, P. J. van Veldhoven, F. W. M. van Otten, T. J. Eijkemans, J. P. Turkiewicz, H. de Waardt, E. J. Geluk, S.-H. Kwon, Y.-H. Lee, R. Nötzel, and M. K. Smit, Nat. Photonics **1**, 589 (2007).
[4]M. T. Hill, M. Marell, E. S. P. Leong, B. Smalbrugge, Y. Zhu, M. Sun, P. J. van Veldhoven, E. J. Geluk, F. Karouta, Y.-S. Oei, R. Nötzel, C.-Z. Ning, and M. K. Smit, Opt. Express **17**, 11107 (2009).
[5]R. F. Oulton, V. J. Sorger, T. Zentgraf, R.-M. Ma, C. Gladden, L. Dai, G. Bartal, and X. Zhang, Nature **461**, 629 (2009).
[6]K. Yu, A. Lakhani, and M. C. Wu, Opt. Express **18**, 8790 (2010).
[7]R. Yan, P. Pausauskie, J. Huang, and P. Yang, Proc. Natl. Acad. Sci. U.S.A. **106**, 21045 (2009).
[8]M. W. Kim and P.-C. Ku, Appl. Phys. Lett. **98**, 201105 (2011).
[9]M. W. Kim and P. C. Ku, Opt. Express **19**, 3218 (2011).
[10]M. P. Nezhad, A. Simic, O. Bondarenko, B. Slutsky, A. Mizrahi, L. Feng, V. Lomakin, and Y. Fainman, Nat. Photonics **4**, 395 (2010).
[11]S.-H. Kwon, J.-H. Kang, C. Seassal, S.-K. Kim, P. Regreny, Y.-H. Lee, C. M. Lieber, and H.-G. Park, Nano Lett. **10**, 3679 (2010).
[12]K. Ding, M. T. Hill, Z. C. Liu, L. J. Yin, P. J. van Veldhoven, and C. Z. Ning, Opt. Express **21**, 4728 (2013).
[13]Y.-J. Lu, J. Kim, H.-Y. Chen, C. Wu, N. Dabidian, C. E. Sanders, C.-Y. Wang, M.-Y. Lu, B.-H. Li, X. Qiu, W.-H. Chang, L.-J. Chen, G. Shvets, C.-K. Shih, and S. Gwo, Science **337**, 450 (2012).
[14]C.-Y. Wu, C.-T. Kuo, C.-Y. Wang, C.-L. He, M.-H. Lin, H. Ahn, and S. Gwo, Nano Lett. **11**, 4256 (2011).
[15]C. Y. Lu, S. W. Chang, S. L. Chuang, T. D. Germann, and D. Bimberg, Appl. Phys. Lett. **96**, 251101 (2010).
[16]Y.-G. Wang, S.-W. Chang, C.-C. Chen, C.-H. Chiu, M.-Y. Kuo, M. H. Shih, and H.-C. Kuo, Appl. Phys. Lett. **99**, 251111 (2011).
[17]Y.-G. Wang, C.-C. Chen, C.-H. Chiu, M.-Y. Kuo, M. H. Shih, and H.-C. Kuo, Appl. Phys. Lett. **98**, 131110 (2011).
[18]U. K. Mishra, P. Parikh, and Y.-F. Wu, Proc. IEEE **90**, 1022 (2002).
[19]S. Nakamura, T. Mukai, and M. Senoh, Appl. Phys. Lett. **64**, 1687 (1994).
[20]S. Li and A. Waag, J. Appl. Phys. **111**, 071101 (2012).
[21]J. C. Carrano and A. J. Maltenfort, Proc. SPIE **4743**, 232 (2002).
[22]Q. Wang, S. Savage, S. Persson, B. Noharet, S. Junique, J. Y. Andersson, V. Liuolia, and S. Marcinkevicius, Proc. SPIE **7216**, 721627 (2009).
[23]C.-C. Chen, C.-H. Chiu, P.-M. Tu, M.-Y. Kuo, M. H. Shih, J.-K. Huang, H.-C. Kuo, H.-W. Zan, and C.-Y. Chang, Jpn. J. Appl. Phys., Part 1 **51**, 04DG02 (2012).
[24]C.-C. Chen, C.-H. Chiu, S.-P. Chang, M. H. Shih, M.-Y. Kuo, J.-K. Huang, H.-C. Kuo, S.-P. Chen, L.-L. Lee, and M.-S. Jeng, Appl. Phys. Lett. **102**, 011134 (2013).
[25]Q. Li, K. R. Westlake, M. H. Crawford, S. R. Lee, D. D. Koleske, J. J. Figiel, K. C. Cross, S. Fathololoumi, Z. Mi, and G. T. Wang, Opt. Express **19**, 25528 (2011).
[26]D. A. Stocker, E. F. Schubert, and J. M. Redwing, Appl. Phys. Lett. **73**, 2654 (1998).

This article is copyrighted as indicated in the article. Reuse of AIP content is subject to the terms at: http://scitation.aip.org/termsconditions. Downloaded to IP: 140.113.38.11 On: Wed, 30 Apr 2014 08:43:22